



Cite this: *Phys. Chem. Chem. Phys.*,
2022, 24, 16900

A temperature programmed desorption study of interactions between water and hydrophobes at cryogenic temperatures

Ryutaro Souda *^a and Tadaaki Nagao ^b

It is considered that hydrophobic solutes dissolve in water *via* the formation of icelike cages in the first hydration shell. However, this conventional picture is currently under debate. We have investigated how hydrophobic species, such as D₂, Ne, Ar, Xe, CH₄, and C₃H₈, interact with water in composite films of amorphous solid water (ASW) based on temperature programmed desorption (TPD). The D₂ and Ne species tend to be incorporated in ASW without being caged, whereas two distinct peaks assignable to the caged species are identifiable for the other solutes examined here. The low-temperature peak is observed preferentially for Ar and CH₄ prior to crystallization. The hydrophobes are thought to be encapsulated in porous ASW films *via* reorganization of the hydrogen bond network up to 100 K; most of them are released in a liquidlike phase that occurs immediately before crystallization at ca. 160 K. The nature of hydrophobic hydration at cryogenic temperature appears to differ from that in normal water at room temperature because the former resembles crystalline ices in the local hydrogen-bond structure rather than the latter. No ordered structures assignable to clathrate hydrates were identified before and after crystallization.

Received 5th April 2022,
Accepted 20th June 2022

DOI: 10.1039/d2cp01580c

rsc.li/pccp

1. Introduction

Hydrophobic hydration is of great importance in many biological phenomena, such as membrane dynamics, drug adsorption, and conformation of proteins and DNA in liquid water.^{1,2} On the other hand, frozen water can form several crystalline compounds under the presence of other molecular substances, known as clathrate hydrates (CHs).³ In addition to fundamental chemistry and physics, interests of CHs arise from their importance in earth and planetary sciences,^{4–7} as well as energy resources and environmental concerns.^{8–10} In order for hydrophobic hydration to occur in both liquid and crystalline water, guest species are encapsulated by water molecules to minimize interactions between water and hydrophobic entities while retaining the water–water hydrogen-bond network. As regards bulk liquid water, the solubility of small nonpolar species is poor because the stable tetrahedral network of hydrogen bonds must be modified to solvate them. Consequently, dissolution of nonpolar species in water is accompanied by a large increase in the heat capacity. Frank and Evans explained this behavior as those water molecules form rigid, icelike structures around

hydrophobic groups.¹¹ According to this “iceberg model”, locally ordered structures resembling those of CHs are expected to be formed. However, experimental determination of the amount of water structuring in the first hydration shell is elusive.¹² Recent experiments and molecular dynamics (MD) simulations reveal that translational and reorientational dynamics of liquid water are slow in the first hydration shell, although the structure of water remains nearly unperturbed relative to that of bulk water.^{13–27}

The formation of CHs from ice also requires breakage and restructuring of the hydrogen-bond network because the arrangement of water molecules in ice is entirely different from that of CHs. The nucleation of crystalline CHs, which is initiated at the gas–ice interface, is expected to be facilitated if the interfacial water species are mobile. Probably, these are the reasons why CHs are formed even in the solid state at a specific temperature and pressure. Consequently, the development of a CH layer on crystalline ice takes a very long time ranging from hours to days. Both water-soluble and water-insoluble species play a role as guest species of CHs, but the structure of CHs collapses into that of liquid water without the support of the solute species. There are three known CH structures, types I, II, and H;³ they are controlled basically by the size of guest species. For example, methane and carbon dioxide form type I CH that consists of a small cage of a pentagonal dodecahedron (5¹²) and a large cage of a

^a Electron Microscopy Analysis Station, National Institute for Materials Science, 1-2-1 Sengen, Tsukuba, Ibaraki 305-0047, Japan. E-mail: SOUDA.Ryutaro@nims.go.jp

^b International Center for Materials Nanoarchitectonics, National Institute for Materials Science, 1-1 Namiki, Tsukuba, Ibaraki 305-0044, Japan

tetradecahedron ($5^{12}6^2$). The type II CH is composed of a small cage of 5^{12} and a large one of hexadecahedron ($5^{12}6^4$). Typical guests of type II CH are N_2 , O_2 , and Ar. Larger guests of type II CHs, such as propane and tetrahydrofuran (THF), generally occupy the large cages. Much smaller solutes like hydrogen are known to be confined in type II CH as well at extremely high pressures typically 220 MPa at 249 K.²⁸ The H_2 molecule can be stored in the CH lattice at lower pressures with the aid of the second guest component like THF.^{29–33} The experimentally-determined hydrogen-to-water molecular ratio reveals that the multiple occupations of H_2 occur in both small and large cages.

The bottleneck of investigating both hydrophobic hydration and CH formation generally arises from the poor miscibility of nonpolar solute species in the liquid water and crystalline ice. This difficulty can be overcome by using co-deposits of water and solutes at low temperatures.^{34–41} Amorphous solid water (ASW) is formed by deposition of pure water molecules at a temperature well below the glass transition temperature ($T_g = 136$ K),⁴² which is followed by crystallization at around $T_c = 160$ K. Therefore, how hydrophobic solutes interact with the liquid and crystalline water can be explored during the heating process of composite ASW films.

In this article, we investigate interactions of water with simple hydrophobes, such as Ne, Ar, Xe, CH_4 , C_3H_8 , and D_2 , together with the role of THF in entrapment of D_2 , based on the experiment of temperature programmed desorption (TPD). It is known that nonpolar species embedded underneath thick ASW films are released explosively during crystallization because they pass through cracks of ice grains (the so-called molecular volcano mechanism).⁴³ The alternative explanation of this phenomenon is that nonpolar species are caged individually by water molecules and then released during the phase transition of water.^{44,45} In any case, TPD experiments provide information about interactions of solute species with water in glassy, liquid, and crystalline phases. Here, attention is focused on how the entrapment and detachment of the additives in water are associated with their sizes or masses to gain more insight into the mechanism of hydrophobic hydration at the molecular level.

2. Experiment

A mirror-finished Pt(111) disc (10 mm \varnothing) was used as a substrate for ASW. It was fixed tightly to a sample holder made of Ta and was inserted into an ultrahigh vacuum (UHV) chamber (a base pressure of 2×10^{-10} torr) through a load-lock system. The surface was cleaned *via* several cycles of Ar^+ sputtering and annealing (~ 1500 K) by electron bombardment from behind. The sample holder was mounted on a Cu rod extended from a closed cycle helium refrigerator. The temperature of the Cu rod close to the sample position was monitored using Au(Fe) chromel thermocouples and was controlled using a digital temperature controller and a cartridge heater. Liquid samples of water and THF were degassed *via* several freeze-pump-thaw cycles; nonpolar gases in Pyrex glass bottles, such

as D_2 , Ne, Ar, Xe, CH_4 , and C_3H_8 , were used without further purification. The gaseous species were placed into the UHV chamber through independent variable leak valves. The surface cleanliness, as well as purity of the deposited films, was monitored *in situ* using time-of-flight secondary ion mass spectrometry (TOF-SIMS) and TPD; formation of the well-ordered Pt(111) surface, as well as the phase transition of ASW into crystalline ices or CHs, was confirmed based on reflection high energy electron diffraction (RHEED).⁴⁶ TPD spectra were obtained using a differentially pumped quadrupole mass analyzer up to the evaporation temperature of multilayered water films (~ 190 K); its housing inlet was movable and approached the sample surface (2–3 mm) during the measurement to minimize the background signal. The sample temperature was ramped at a rate of 5 K min^{-1} for each measurement using a cartridge heater and a digital temperature controller. A monolayer (ML) of the ASW film is formed by exposure of 2 L of H_2O molecules at the substrate temperature of 100 K.⁴ The composite ASW films were characterized here based on the exposure of gaseous species rather than their exact thickness because of the ambiguity arising from the sticking probability of lighter species.

3. Experimental results

3.1 Rare gases

Fig. 1 shows TPD spectra of H_2O ($m/z = 18$) and Ne (22) desorbed from the ASW film, each co-deposited at 1×10^{-6} torr for 100 seconds (100 Langmuir (L)) at the substrate temperature of 30 K. The detachment of water commences at around 140 K and a characteristic shoulder appears at *ca.* 160 K because of crystallization. The desorption rate of water molecules is peaked at *ca.* 180 K. These results are fundamentally

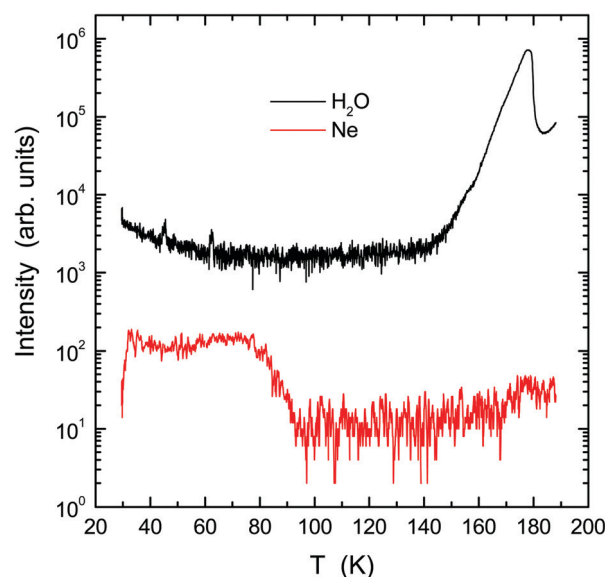


Fig. 1 TPD spectra of H_2O ($m/z = 18$) and Ne (22) from the composite film prepared *via* co-deposition (100 L each) at 30 K onto the Pt(111) substrate. Temperature was ramped at a rate of 5 K min^{-1} .

identical to those obtained using pure ASW films.⁴⁶ The co-deposited Ne species are incorporated in the ASW film interior, as evidenced by a broad TPD spectrum of Ne, but they are released almost completely up to 90 K.

TPD spectra of Ar are displayed in Fig. 2(a), together with a typical water TPD spectrum. The film was formed by exposing the Pt(111) substrate to H₂O and Ar gas mixtures at 30 K with different proportions; red for 100 L (1×10^{-6} torr for 100 s) each and green for 100 L H₂O and 1 L (1×10^{-7} torr for 100 s) Ar. Also shown in Fig. 2(b) are TPD spectra of Ar from co-deposited ASW films (100 L each) at different substrate temperatures (60–80 K). In this temperature range, the H₂O molecule sticks to the surface with a probability of unity. The film is characterized by a microporous structure when deposited at temperatures below 70 K.^{47,48} For the co-deposited film at 30 K, a broad Ar peak with an extended tail is followed by sharp peaks at 150 and 157 K before the water desorption rate changes at *ca.* 160 K because of crystallization. It should be noted that no such doublet TPD peak was observed when Ar was pre-adsorbed onto graphene-covered Pt(111) and then buried underneath the ASW film.⁴⁹ A huge peak of Ar at 40 K results from weakly physisorbed species trapped in interstices of ASW or adsorbed onto the pore wall surface. In this respect, the monolayer TPD peak from the nonporous ASW film is known to occur at considerably low temperature,⁵⁰ indicating that the interaction of Ar with ASW is noticeably weaker than

the interaction with graphene. In the present study, however, the TPD peak of 1 L Ar (60 K) occurs at a temperature rather higher than that of the monolayer Ar on graphene (45 K). The broad peak is followed by an extended tail, but no such behaviors are observed for Ar on graphene and nonporous ASW film surfaces.⁵⁰ These results strongly suggest that the broad peak and tail arise from Ar at higher coordination sites of water characteristic of the porous ASW film.

The TPD spectra of Ar, designated as peaks A, B, and C, originate from trapped species that are released before (A and B) and after (C) crystallization of water. The origin of the high temperature peak B might be explained in terms of the molecular volcano mechanism.⁴³ However, it should be noted that most of the Ar in peak B is released before crystallization occurs at $T_c = 160$ K, where not only the desorption rate of water but also the electron diffraction pattern changes because of the formation of ice grains. Moreover, it is apparent that peak A at 150 K has nothing to do with ice nucleation. These behaviors clearly show that Ar is released from liquidlike water that is formed prior to crystallization. Therefore, we consider that these peaks originate from dehydration of caged species rather than the molecular volcano *via* crack propagation induced by crystallization. Indeed, the fact that the intensity of peak A relative to peak B is independent of the initial Ar content strongly suggests that they have the same origin, resulting from individually trapped species in water cages rather than condensed Ar species embedded underneath thick water layers. Consequently, the doublet TPD peaks of Ar imply that two distinct hydration states exist in ASW or liquidlike water formed at T_g . Only a very small amount of Ar survives the phase transition. Probably, the Ar species trapped in grain boundaries lead to peak C. With increasing substrate temperature during deposition, the amount of Ar trapped in the ASW film is reduced as shown in Fig. 2(b). The intensity of peak B decreases relative to that of peak A at higher deposition temperature while keeping their peak positions constant.

In Fig. 3 are compared TPD spectra of Xe (1 and 100 L) that is co-deposited with H₂O (100 L) at 30 K. The intensity of peak B is much higher than that of peak A in contrast to Ar TPD, although their relative intensities are almost independent of the initial Xe content. When the amount of initially trapped Xe becomes much smaller than that of the matrix H₂O molecules, the broad peak from condensed Xe atoms at ~ 80 K is extinguished, together with the extended tail. It might be presumed that the hydrates are formed such that the rare-gas species are included in the ASW film interior during pore collapse. However, the pore collapse occurs at a higher temperature (120–140 K)⁴⁸ than the thermal desorption temperature of weakly-physisorbed Xe species (80–90 K). Consequently, the Xe atoms caged individually by water molecules at the porous ASW film surface result in peaks A and B, whereas the 2D or 3D Xe species condensed on the pore wall surface or in the interstice are thought to be responsible for the broader components.

To summarize the results for rare gas atoms, the structure of TPD spectra is found to be strongly dependent on the size or mass of the trapped species. For Ar and Xe, two distinct

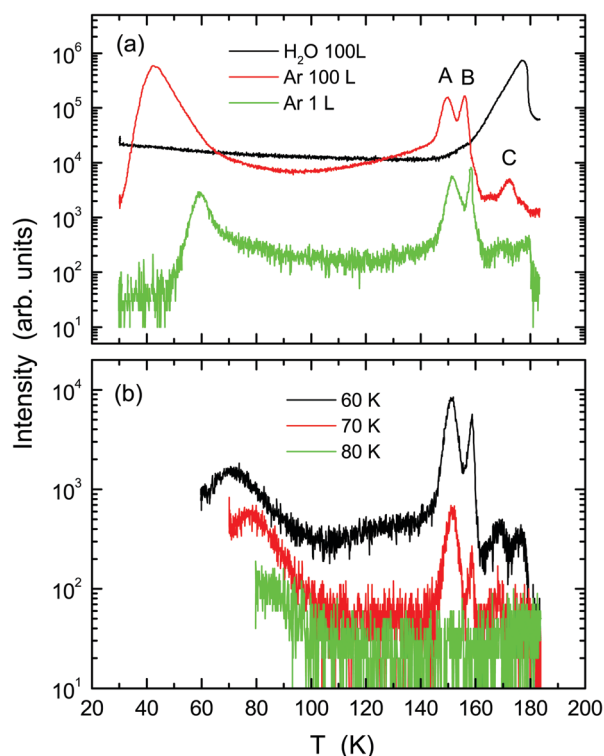


Fig. 2 (a) TPD spectra of H₂O and Ar ($m/z = 40$) from the composite films prepared by co-deposition of H₂O (100 L) and Ar (1 and 100 L) onto the Pt(111) substrate at 30 K. Also shown in (b) are the TPD spectra of Ar from the composites of H₂O and Ar (100 L each) at different substrate temperatures.

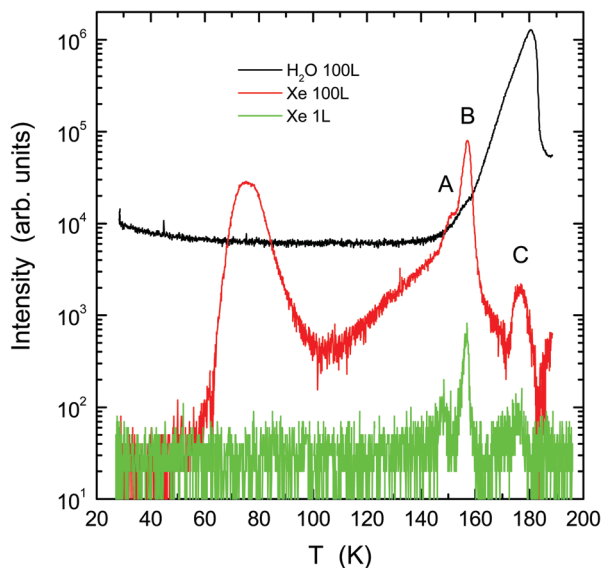


Fig. 3 TPD spectra from the composite films of water and Xe ($m/z = 132$) prepared by co-deposition of H₂O (100 L) and Xe (1 and 100 L) onto the Pt(111) substrate at 30 K.

hydration states are recognizable as separated peaks A and B. The low-temperature peak A, which is more abundant for Ar than Xe, is ascribable to smaller cages of water molecules that confine smaller species preferentially. In the case of Ne, however, the extended tail occurs without any peaks because no hydrates or caged species are formed in ASW and the liquidlike water.

3.2 Hydrocarbons

The interactions of hydrocarbons with ASW are also investigated in terms of the solute size. In Fig. 4 are compared TPD

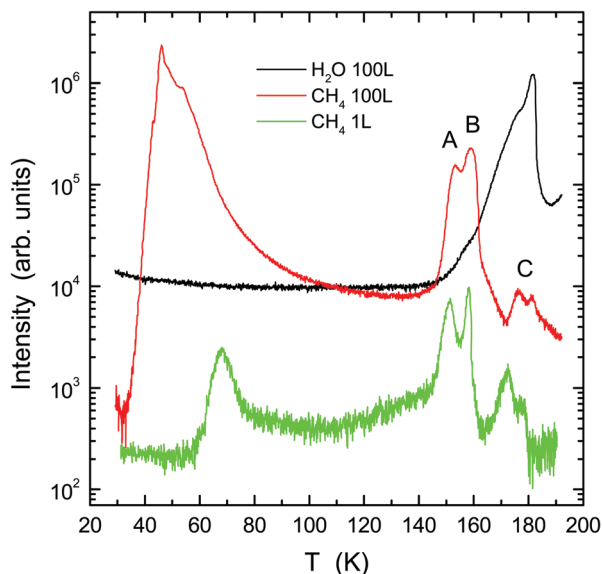


Fig. 4 TPD spectra of CH₄ ($m/z = 15$) from the composite films prepared by co-deposition of H₂O (100 L) and CH₄ (1 and 100 L) onto the Pt(111) substrate at 30 K.

spectra of CH₄ (1 and 100 L) co-deposited with H₂O (100 L) at the substrate temperature of 30 K. The doublet peaks of the hydrated CH₄ species are recognizable before water crystallizes at 160 K. The relative intensity of peak A to B is almost independent of its initial content although each peak is broadened to some extent at higher CH₄ content. The huge peak at *ca.* 45 K originates from 2D or 3D islands of the condensed CH₄ molecules, whereas the corresponding peak is sharpened and shifted to a higher temperature (65 K) at a smaller CH₄ content. The latter is ascribable to more scattered species in direct contact with the surface, as inferred from a much smaller amount of the CH₄ species relative to water. It is known that TPD spectra of CH₄ adsorbed on graphene and nonporous ASW films peak at temperatures well below 60 K.⁵⁰ Therefore, the occurrence of the peak at 65 K, as well as the extended tail, suggests that the CH₄ molecules tend to be trapped transiently in the ASW film interior or on pore wall surfaces. They are expected to develop into caged (hydrated) species at higher temperatures. Consequently, the evolutions of the low-temperature peak (65 K), extended tail, and high-temperature doublet peaks indicate that the local environments of the CH₄ molecule change during the heating process.

Fig. 5 displays TPD spectra of propane (1 and 100 L) co-deposited with H₂O (100 L) at 30 K. Peak A becomes much smaller than peak B in intensity irrespective of the initial propane content. The propane is condensed in 3D islands at higher exposure to form a TPD peak at 95 K, but this species is absent when the propane content is low (1 L), indicating that all propane additives evolve into hydrated species. These behaviors contrast with those of CH₄ but are fundamentally identical to those of Xe. Thus, a larger (or heavier) solute species that can withstand higher temperatures evolve into hydrated species more efficiently.

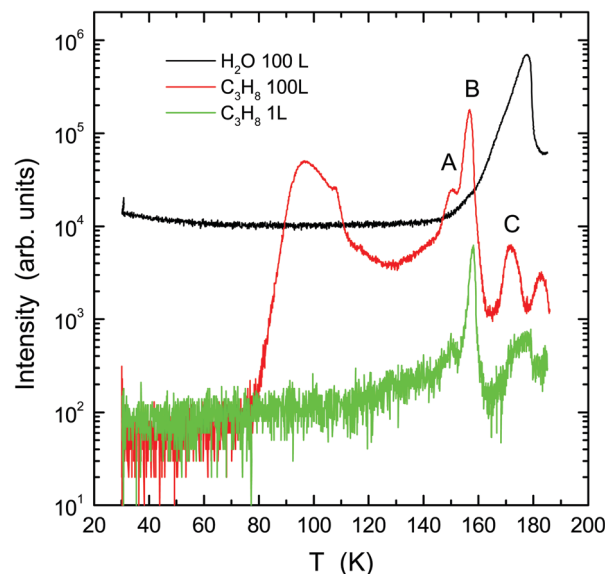


Fig. 5 TPD spectra of C₃H₈ ($m/z = 29$) from the composite films prepared by co-deposition of H₂O (100 L) and C₃H₈ (1 and 100 L) onto the Pt(111) substrate at 30 K.

3.3 Deuterium

Smaller (or lighter) solute species are of interest in terms of hydration, as inferred from the apparently distinct behaviors of Ne relative to Ar and Xe. The same is expected to occur for hydrogen or deuterium interacting with water. Fig. 6 shows typical TPD spectra of H₂O and D₂ molecules. The ASW film is formed by deposition of 100 L H₂O at 30 K and then exposed to a different amount of the D₂ molecule (100 L: 1×10^{-6} torr for 100 s; 1000 L: 1×10^{-5} torr for 100 s) at the same temperature. The physisorbed species in the near surface region are expected to be released in the lower temperature range. In fact, a high-temperature component evolves at higher exposure because the D₂ molecules can penetrate the interior of the porous ASW film. In any case, hydrated D₂ species are not formed, as evidenced by the absence of the sharp peaks. We consider that the broad components of the D₂ and Ne TPD spectra are fundamentally identical to the extended tails observed using Ar and CH₄. The presence of the tail at higher D₂ exposure indicates that higher coordination sites formed in the interior of the porous ASW film play a role in the transient entrapment of the D₂ molecule. In this respect, it is known that the heavier species, such as *n*-hexane, formaldehyde, and acetone,⁵¹ adsorbed onto porous ASW films evolve into well-defined hydrates in the interior, providing a significant contrast to the D₂ adspecies.

In Fig. 7(a) are displayed TPD spectra of D₂ and H₂O (100 L each) co-deposited at 30 K. Results are fundamentally identical to those observed in Fig. 6 at higher D₂ exposure because the molecules incorporated in the ASW film interior are released gradually over a wide temperature range. In this respect, how D₂ interacts with THF and the water-THF mixture is of interest because THF is known to facilitate the H₂ confinement in type II CHS.^{29–33} As shown in Fig. 7(b), the amount of D₂ molecules incorporated in the THF film (prepared by co-deposition of

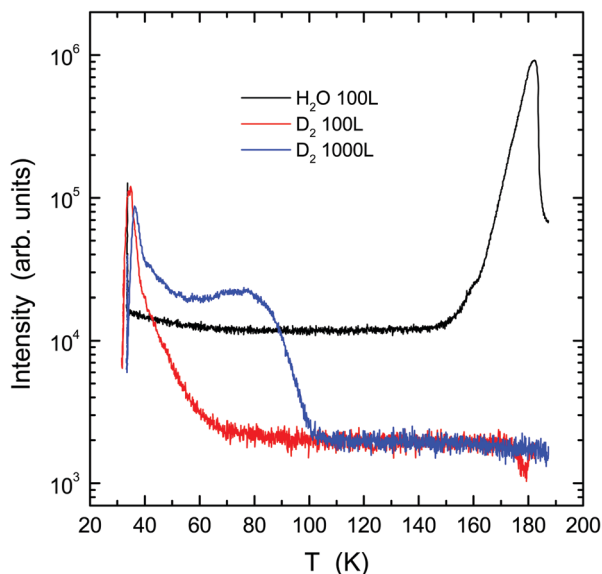


Fig. 6 TPD spectra of H₂O and D₂ ($m/z = 4$) from the ASW film (formed by deposition of 100 L H₂O at 30 K) after exposure to 100 and 1000 L D₂ molecules at 30 K.

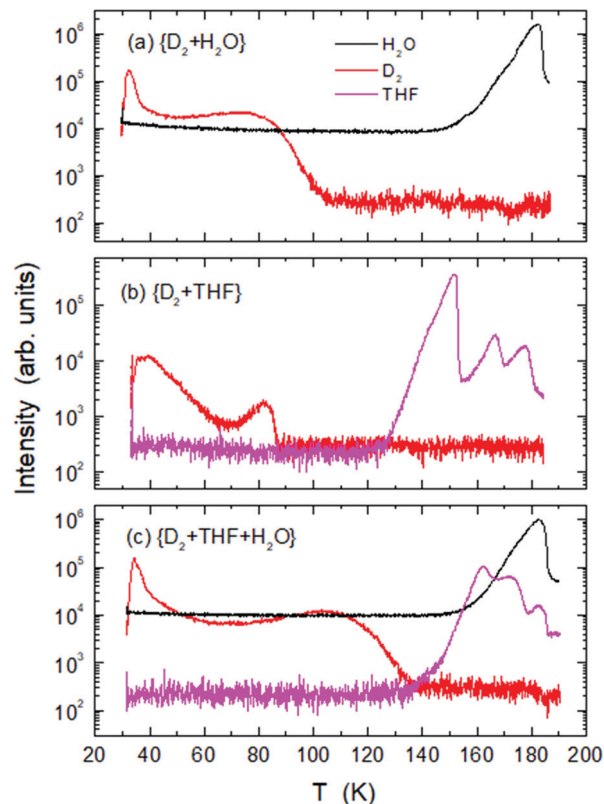


Fig. 7 TPD spectra from binary composite films of (a) D₂ and H₂O and (b) D₂ and THF are compared with those from a ternary composite film of (c) D₂, THF, and H₂O. The molecules (100 L each) were co-deposited onto the Pt(111) substrate at 30 K.

each molecule at 100 L) is small relative to that in the ASW film, suggesting that THF alone has no appreciable effects on the uptake of the D₂ molecule relative to the pure ASW film. However, the D₂ entrapment is improved considerably in the ternary mixture of D₂, THF, and H₂O (100 L each), as shown in Fig. 7(c). The D₂ molecule tends to stay in the mixed film interior at a higher temperature (140 K) than in the binary composite film (110 K). It is thus suggested that THF additives improve the entrapment of D₂ although no sharp hydrate peaks occur at 150–160 K. Consequently, well-defined hydrates of D₂ molecules are formed neither in the pure ASW film nor in the mixed water-THF film prepared *via* co-deposition of the molecules at cryogenic temperatures.

4. Discussion

Based on the experimental facts described above, we can deduce how the hydrophobic solute species interact with ASW to form hydrates. The additives at smaller content (1 L) are expected to interact individually with water molecules in the interstice or on the pore-wall surface of ASW, although they are not caged immediately after deposition at 30 K because water molecules are arranged in random orientations. In fact, a large number of hydrogen bond imperfections (*i.e.*, unpaired hydrogen bonds) are known to exist between water molecules on the

porous ASW film surface, as revealed from the TOF-SIMS experiment.⁵² The water cluster ions, $D^+(D_2O)_n$, are sputtered efficiently from a porous D_2O film deposited at 15 K; intensities of the cluster ions decrease gradually in the temperature range of 50–100 K. This behavior is ascribable to the reorientation of water molecules to recover the hydrogen bond network. On the other hand, surface diffusion of water commences at a higher temperature (110–120 K), as revealed from the uptake of the water monolayer into porous media.⁵³ From these facts, we consider that the pore collapse at *ca.* 120 K is induced by the surface diffusion of water molecules. Therefore, the absence of the physisorbed species in the TPD spectra of the diluted mixture of Xe or propane with water at $T < 100$ K is not simply ascribable to the entrapment of solutes *via* the collapse of the inner pores. Probably, the hydrophobic species are encapsulated during the reorientation of surrounding water molecules to recover the hydrogen bond network. The encapsulation of lighter species, such as Ar and CH_4 , is less efficient than the heavier species because the formers are released at lower temperatures before caging is completed even at a small exposure (1 L). In contrast to such weakly physisorbed species (*i.e.*, precursors to hydrates), the gas-phase Ar atoms do not evolve into hydrates during co-deposition with water at 80 K, as shown in Fig. 2(b). Consequently, the physisorbed solute species are encapsulated preferentially by coadsorbed water molecules in the temperature range of 50–100 K, which is followed by their uptake in the ASW film interior not only *via* surface diffusion (*i.e.*, pore collapse) at $T > 110$ –120 K but also *via* translational diffusion in the bulk above $T_g = 136$ K. In fact, no hydrates are formed on the surface of ASW films prepared by deposition of water molecules at higher temperatures (~ 100 K) because hydrogen bond imperfections to develop into microscopic cages are absent. The entrapment difference appears to exist between the atomic and molecular species with comparable masses. In contrast to D_2 , no He atoms are incorporated in the ASW film (not shown) because gas phase species without physisorption are not trapped by water molecules. This situation resembles that for Ar deposited at 80 K. The CH_4 molecules form well-defined hydrates, but the heavier Ne atoms are not encapsulated by water. This behavior might be explained by the presence of a weak $CH \cdots O$ hydrogen bond between methane and water.

It might be presumed that the sharp peaks A and B are indicative of the formation of crystalline CHs. However, no long-range ordering is identified in electron diffraction patterns during the heating process of the composite films till ice Ic is formed at $T_c = 160$ K.⁵⁴ The results for crystallization kinetics are fundamentally identical to those using pure ASW films. This is reasonable because most of the nonpolar additives are released in the liquidlike phase prior to crystallization as demonstrated here. A small amount of the trapped solute species might evolve into crystalline CHs at grain boundaries, though they are not clearly distinguishable from ice Ic based on the diffraction pattern. As demonstrated here, the hydrated species in the grain boundaries are recognizable as peak C in TPD. However, the long-range ordering of molecules, or a

particular structure type of CHs, must be determined from diffraction studies.^{37–39} The spectroscopic data are useful in some cases for the recognition of local structure evolutions in amorphous phases and dynamics around individual guest species. In this respect, the development of CHs from the co-deposits of water and various solute species has been reported based on Raman, infrared, and NMR studies at cryogenic temperatures.^{34–41} Hallbrucker suggested that CHs resulting from vapor-deposited ASW necessitate the coexistence of a large amount of crystalline ice to stabilize them.³⁹ This is fundamentally consistent with the present result using much thinner films. Using NMR spectroscopy combined with X-ray powder diffraction, Ripmeester and coworkers found that hyperquenched glasses of aqueous THF solutions undergo phase separation into domains of crystalline THF and ice Ic before crystallization into CH is initiated;³⁵ a large-scale growth of crystalline CH is associated with a reduction of crystalline THF and ice Ic domains above 150–160 K. The ordering of Xe and water co-deposits into CHs commences at 140 K, although the process is not complete until a temperature of 180 K is reached.^{37,38} On the other hand, Devlin and coworkers claimed that amorphous composites of polar aprotic species with water form CHs at temperatures as low as 130 K.³⁴ Consequently, the local ordering of water molecules around hydrophobic solute species is evidenced by the vibrational and NMR spectroscopies, although long-range ordering of CHs is not identified in both X-ray powder diffraction and RHEED before water crystallization occurs at *ca.* 160 K.

The fact that the hydrophobic solutes enhance the local ordering of liquidlike water reminds us of the iceberg model.¹¹ For liquid water at room temperature, however, the effect of hydrophobes on the structural dynamics of water molecules seems to be controversial.^{12–27} The neutron diffraction study of water in methane–water solution at 18 °C and 180 bar rather concluded that the structure is marginally less tetrahedral than that in pure water at the same temperature and pressure.¹² Although the exact structure of water in the first solvation shell is hardly determined experimentally, computer simulations reveal that ordered aggregates of water molecules can be formed.^{13,22} On the other hand, there are many reports showing that the dynamics of the solvating water around hydrophobic species is slower than the dynamics of bulk water, which is not necessarily attributed to the structural change in water.^{19–21} Currently, the iceberg picture is rather supported from the dynamical point of view for normal liquid water: the water molecules around hydrophobic groups retain a liquidlike structure although their dynamics would be icelike, thereby explaining why hydrophobic icebergs have not been observed using structural methods.

The conflicting results of hydrophobic hydration of water between room temperature and cryogenic temperature are likely to be elucidated in terms of polyamorphism;⁵⁵ the liquidlike water formed at T_g is known as a distinct liquid, termed as low density liquid (LDL). It is a tetrahedrally-structured liquid with a local structural resemblance to crystalline ice rather than normal liquid water.⁵⁶ Therefore, icelike cages are expected to be formed locally to incorporate nonpolar solute species in

LDL. However, it should be noted that such caged species do not evolve directly into crystalline CHs, as evidenced by the fact that hydrated species are released from the liquidlike water formed before crystallization. This result implies the occurrence of the liquid–liquid (L–L) phase transition: LDL transforms into the other liquid phase, probably normal water, immediately before crystallization.⁵⁷ The icelike cages of water molecules are likely to collapse during the L–L transition so that most of the hydrated nonpolar species are released. The normal liquid water, if any, undergoes immediate crystallization because of its instability at cryogenic temperatures. This L–L transition hypothesis has been inferred from the interactions of water with alkali halides at cryogenic temperatures.^{57,58} For example, LiCl adspecies are incorporated in the film interior at around T_c rather than T_g because aqueous solutions of alkali halides result from normal water formed *via* the L–L transition rather than LDL having a crystal-like local structure.

The large-scale growth of CHs generally proceeds at $T > T_c$ on the crystalline ice surface during interactions with hydrophobes. This behavior is likely to be associated with premelting of ice. It is known that the surface of ice Ic grains behaves like a liquid at $T > 150$ K in terms of the uptake of LiCl⁵⁸ so that the hydrophobic species can also be incorporated at the interface to create CH films. Similarly, premelting of ice Ih is likely to occur at temperatures below its melting point (273 K).⁵⁹ This behavior is likely to be associated with the gradual growth of crystalline CHs at the ice surface under high pressures.

The peaks A and B of solute species observed in the TPD spectra might imply the formation of clathrate-like cages, although no long-range ordering of crystalline CHs is identifiable below $T_c = 160$ K. The fact that peak B is commonly observed irrespective of the solute size strongly suggests that any sized cages (probably disordered) can be formed to encapsulate the solute species in LDL. In contrast, peak A is likely to result from a specifically structured cage because it is observed preferentially for small solute species. Despite this tendency, however, no well-defined hydrate peaks of Ne are recognizable, suggesting that Ne is too small to be caged. It is likely that Ne passes through the hydrogen-bond network of water molecules to form solutions with ASW. This behavior might be associated with the thermodynamic instability of Ne CHs.⁶⁰ The same is expected to occur for the interaction of water with deuterium. It is revealed that type II CHs of hydrogen can be formed under extremely high pressure²⁸ to accommodate multiple hydrogen molecules in the cages, although hydrogen is diffusive in the interstice of crystalline ice Ih.⁶¹ As suggested here, no local cages of water molecules are expected to be formed during interactions with D₂. However, the second solutes like THF create local cages of water molecules so that a larger amount of hydrogen can be incorporated into the openings. Most of the D₂ molecule is released up to 140 K because liquidlike water (LDL) evolves in bulk as a result of the glass–liquid transition.

5. Conclusion

Interactions of hydrophobes with water were investigated through their hydration and dehydration behaviors as a

function of temperature. Three distinct states of nonpolar species are identified in the TPD spectra during the heating process of composite films formed at 30 K, *i.e.*, condensed species forming 2D or 3D islands, scattered species in direct contact with the water molecules, and hydrated species confined individually in cages of water molecules. They are distinguishable based on the TPD spectra because the desorption temperature of the solute species is a good experimental measure of the binding site energies that are controlled by the local environments of water molecules. The caged species form well-defined TPD peaks at 150–160 K. The larger the size of the solutes, the easier the formation of hydrated species. Specifically, solid solutions are formed for D₂ without being caged in ASW and water–THF composites; mobile molecules in the film interior can be released continuously from the surface. The same occurs for Ne in ASW. On the other hand, two distinct hydrates are recognizable for Ar, Xe, CH₄, and C₃H₈ in ASW, as revealed from the occurrence of the doublet TPD peaks. The low-temperature peak might be associated with smaller cages because it is more abundant for the smaller Ar and CH₄ species. From a comparison between TPD and previous TOF-SIMS results, it is suggested that the solute species are caged during the reorientation of water molecules to recover hydrogen bond networks on the pore wall surface at a temperature below 100 K. Then, hydrates are finally formed in the interior of ASW and LDL. However, no long-range ordering of crystalline CHs is identifiable from the diffraction patterns before and after crystallization into ice Ic, indicating that the caged species are formed in the amorphous phase. Most of the hydrated species are released during the L–L transition immediately before crystallization. The hydrophobic hydration at cryogenic temperature appears to be distinct from that in normal water in terms of the icelike cage formation because LDL is the tetrahedrally-structured liquid having a local structural resemblance to crystalline ices.

Conflicts of interest

There are no conflicts to declare.

Acknowledgements

This research was partly funded by the Japan Society for the Promotion of Science through a Grant-in-Aid for Scientific Research (C), No. 22540339.

References

- 1 J. G. Davis, K. P. Gierszal, P. Wang and D. Ben-Amotz, *Nature*, 2012, **492**, 582–585.
- 2 P. Ball, *Chem. Rev.*, 2008, **108**, 74–108.
- 3 E. D. Sloan and C. A. Koh, *Clathrate Hydrates of Natural Gases*, 3rd edn, CRC Press, Boca Raton, FL, 2008.
- 4 D. Gautier, F. Hersant, O. Mousis and J. I. Lunine, *Astrophys. J.*, 2001, **550**, L227–L230.

- 5 M. T. Mellon, *Icarus*, 1996, **124**, 268–279.
- 6 N. Iro, D. Gautier, F. Hersant, D. Bockelee-Morvan and J. I. Lunine, *Icarus*, 2003, **161**, 511–532.
- 7 P. Englezos, *Ind. Eng. Chem. Res.*, 1993, **32**, 1251–1274.
- 8 Y. F. Makogon, *J. Nat. Gas Sci. Eng.*, 2010, **2**, 49–59.
- 9 K. C. Hester and P. G. Brewer, *Ann. Rev. Mar. Sci.*, 2009, **1**, 303–327.
- 10 K. A. Kvenvolden, *Org. Chem.*, 1995, **23**, 997–1008.
- 11 H. S. Frank and M. W. Evans, *J. Chem. Phys.*, 1945, **13**, 507–532.
- 12 P. Buchanan, N. Aldiwan, A. K. Soper, J. L. Creek and C. A. Koh, *Chem. Phys. Lett.*, 2005, **415**, 89–93.
- 13 N. Galamba, *J. Phys. Chem. B*, 2013, **117**, 2153–2159.
- 14 X. Wu, W. Lu, L. M. Streacker, H. S. Ashbaugh and D. Ben-Amotz, *Angew. Chem., Int. Ed.*, 2018, **57**, 15133–15137.
- 15 J. Gradolnik, F. Merzel and F. Avbelj, *Proc. Natl. Acad. Sci. U. S. A.*, 2017, **114**, 322–327.
- 16 F. Merzel and F. Avbelj, *Biochim. Biophys. Acta, Gen. Subj.*, 2020, **1864**, 129537.
- 17 S. Strazdaite, J. Versluis, E. H. G. Backus and H. J. Bakker, *J. Chem. Phys.*, 2014, **140**, 054711.
- 18 P.-L. Chau and R. L. Mancera, *Mol. Phys.*, 1999, **96**, 109–122.
- 19 J. Qvist and B. Halle, *J. Am. Chem. Soc.*, 2008, **130**, 10345–10353.
- 20 D. Laage, G. Stirnemann and J. T. Hynes, *J. Phys. Chem. B*, 2009, **113**, 2428–2435.
- 21 Y. L. A. Rezus and H. J. Bakker, *Phys. Rev. Lett.*, 2007, **99**, 148301.
- 22 J. Grabowska, A. Kuffel and J. Zielkiewicz, *J. Phys. Chem. B*, 2021, **125**, 1611–1627.
- 23 C. A. Koh, R. P. Wisbey, X. P. We and R. E. Westacott, *J. Chem. Phys.*, 2000, **113**, 6390–6397.
- 24 D. Laage, G. Stirnemann and J. T. Hynes, *J. Phys. Chem. B*, 2009, **113**, 2428–2435.
- 25 J. G. Davis, K. P. Gierszal, P. Wang and D. Ben-Amotz, *Nature*, 2012, **491**, 582–585.
- 26 Y. L. A. Rezus and H. J. Bakker, *Phys. Rev. Lett.*, 2007, **99**, 148301.
- 27 J. Qvist and B. Halle, *J. Am. Chem. Soc.*, 2008, **130**, 10345–10353.
- 28 W. L. Mao, H.-K. Mao, A. F. Goncharov, V. V. Struzhkin, Q. Guo, J. Hu, J. Shu, R. J. Hemley, M. Somayazulu and Y. Zhao, *Science*, 2002, **297**, 2247–2249.
- 29 L. J. Florusse, C. J. Peters, J. Schoonman, K. C. Hester, C. A. Koh, S. F. Dec, K. N. Marsh and E. D. Sloan, *Science*, 2004, **306**, 469–471.
- 30 H. Lee, J. W. Lee, D. Y. Kim, J. Park, Y.-T. Seo, H. Zeng, I. L. Moudrakovski, C. I. Ratcliff and J. A. Ripmeester, *Nature*, 2005, **434**, 743–746.
- 31 T. A. Strobel, K. C. Hester, C. A. Koh, A. K. Sum, K. T. Miller and E. D. Sloan, *Chem. Phys. Lett.*, 2009, **478**, 97–109.
- 32 P. D. Gorman, N. J. English and J. M. D. MacElroy, *Phys. Chem. Chem. Phys.*, 2011, **13**, 19780–19787.
- 33 H. Cao, N. J. English and J. M. D. MacElroy, *J. Chem. Phys.*, 2013, **138**, 0945507.
- 34 V. Buch, J. P. Devlin, I. A. Monreal, B. Jagoda-Cwiklik, N. Uras-Aytemiz and L. Cwiklik, *Phys. Chem. Chem. Phys.*, 2009, **11**, 10245–10265.
- 35 C. A. Tulk, Y. Ba, D. D. Klug, G. McLaurin and J. A. Ripmeester, *J. Chem. Phys.*, 1999, **110**, 6475–6483.
- 36 B. Chazallon, A. O. Oancea, B. Capoen and C. Focsa, *Phys. Chem. Chem. Phys.*, 2008, **10**, 702–712.
- 37 I. L. Moudrakovski, A. A. Sanchez, C. I. Ratcliffe and J. A. Ripmeester, *J. Phys. Chem. B*, 2001, **105**, 12338–12347.
- 38 H. Nakayama, D. D. Klug, C. I. Ratcliffe and J. A. Ripmeester, *Chem. – Eur. J.*, 2003, **9**, 2969–2973.
- 39 A. A. Hallbrucker, *Angew. Chem., Int. Ed. Engl.*, 1994, **33**, 691–692.
- 40 J. Ghosh, R. R. Methikkalam, R. G. Bhun, G. Ragupathy, N. Choudhary, R. Kumar and T. Pradeep, *Proc. Natl. Acad. Sci. U. S. A.*, 2019, **116**, 1526–1531.
- 41 J. Ghosh, R. G. Bhui, G. Vishwakarma and T. Pradeep, *J. Chem. Phys. Lett.*, 2020, **11**, 26–32.
- 42 R. Souda, *Phys. Rev. Lett.*, 2004, **93**, 235502.
- 43 R. S. Smith, C. Huang, E. K. L. Wong and B. D. Kay, *Phys. Rev. Lett.*, 1997, **79**, 909–912.
- 44 T. Livneh, L. Room and M. Asscher, *Surf. Sci.*, 1996, **351**, 250–258.
- 45 Y. Lilach and M. Asscher, *J. Chem. Phys.*, 2002, **117**, 6730–6736.
- 46 R. Souda and T. Aizawa, *J. Phys. Chem. C*, 2018, **122**, 28094–28104.
- 47 K. P. Stevenson, G. A. Kimmel, Z. Dohnalek, R. S. Smith and B. D. Kay, *Science*, 1999, **283**, 1505–1507.
- 48 G. A. Kimmel, K. P. Stevenson, Z. Dohnalek, R. S. Smith and B. D. Kay, *J. Chem. Phys.*, 2001, **114**, 5284–5294.
- 49 R. A. May, R. S. Smith and B. D. Kay, *J. Chem. Phys.*, 2013, **138**, 104501.
- 50 R. S. Smith, R. A. May and B. D. Kay, *J. Phys. Chem. B*, 2016, **120**, 1979–1987.
- 51 R. Souda, *Appl. Surf. Sci.*, 2015, **357**, 1809–1815.
- 52 R. Souda, H. Kawanowa, M. Kondo and Y. Gotoh, *J. Chem. Phys.*, 2003, **119**, 6194–6200.
- 53 R. Souda, *J. Phys. Chem. C*, 2011, **115**, 8136–8143.
- 54 R. Souda and T. Aizawa, *J. Phys. Chem. C*, 2019, **123**, 27055–27063.
- 55 O. Mishima and H. E. Stanley, *Nature*, 1998, **396**, 329–335.
- 56 J. L. Finney, A. Hallbrucker, I. Kohl, A. K. Soper and D. T. Bowron, *Phys. Rev. Lett.*, 2002, **88**, 225503.
- 57 R. Souda, *J. Chem. Phys.*, 2006, **125**, 182203.
- 58 R. Souda, *J. Phys. Chem. C*, 2017, **121**, 12199–12205.
- 59 M. Muro, M. Harada, T. Hasegawa and T. Okada, *J. Phys. Chem. C*, 2012, **116**, 13296–13301.
- 60 D. Londono, J. L. Finney and W. F. Kuhs, *J. Chem. Phys.*, 1992, **97**, 547–552.
- 61 H. L. Strauss, Z. Chen and C.-K. Loong, *J. Chem. Phys.*, 1994, **101**, 7177–7180.